

# Wind retrieval capability of rotating, range-gated, fanbeam spaceborne scatterometer

Chung-Chi Lin<sup>\*a</sup>, Ad Stoffelen<sup>\*\*b</sup>, Joost de Kloe<sup>\*\*b</sup>, Volkmar Wismann<sup>\*\*\*c</sup>, Sven Bartha<sup>\*\*\*\*d</sup>, Hans-Reiner Schulte<sup>\*\*\*\*d</sup>

<sup>a</sup>European Space Agency (ESTEC), <sup>b</sup>Royal Netherlands Meteorological Institute,

<sup>c</sup>Institute for Applied Remote Sensing, <sup>d</sup>Astrium GmbH

## ABSTRACT

The primary mission of a wind scatterometer is to determine wind speed and direction over the ocean. This is achieved by performing a set of radar cross-section measurements at different azimuth view-angles over the resolution cell, and inverting the backscatter model, a so-called geophysical model function (GMF), to extract the wind information using the azimuth anisotropy of the radar backscatter by sea-surface in presence of wind. A new concept of rotating fanbeam radar was introduced which operates in C-band. The present paper describes an analysis of the new concept by means of wind retrieval simulations and an investigation of advanced features such as multi-beam, dual-polarisation, dual-frequency and polarimetric capabilities in improving the wind retrieval accuracy. End-to-end simulations of the complete system are performed starting from wind-fields which are sampled by the scatterometer model. The simulated radar echos are then converted to sets of backscattering coefficients (sigma-naught) which are inverted to obtain again the wind-fields containing measurement errors and noise. The performance of the system is assessed by analysing the quality of retrieved wind as functions of the instrument configuration and characteristics (parameters).

**Keywords:** Wind scatterometer, ocean wind, satellite, radar simulations, wind retrieval performance

## 1. ROTATING FANBEAM SCATTEROMETER CONCEPT

Windsatellite data are operationally assimilated into numerical weather prediction (NWP) models at a number of meteorological centers and are becoming indispensable as part of the global observation system. E.g., 4D-Var assimilation of scatterometer data at ECMWF has demonstrated positive impacts on tropical cyclone analyses and forecasts over the Atlantic<sup>1</sup>. Two essential requirements for any scatterometers operating in the future are:

- (1) High quality (accurate) wind data derived from the system in order to enable further positive impacts on the forecasts of highly sophisticated, steadily improving NWP models;
- (2) Frequent global coverage, requiring a very large instantaneous swath, for covering the needs of very short-range forecasting (up to 24 hrs), in particular for storm-track predictions and off-shore applications.

A new scatterometer concept<sup>2</sup> was studied under ESA which attempts to meet the above two requirements, yet simple and robust enough to permit a cost-effective system implementation. To recall the basic idea of the new concept, the working principle of the Rotating Fanbeam SCATterometer (RFSCAT) is illustrated in Fig. 1.

A wide-fanbeam antenna rotates slowly around the vertical axis such that its footprint sweeps a fat donut-shape on the Earth surface. Combined with the spacecraft motion of approx. 7 km/s ground-speed, large overlaps are produced by the successive sweeps. A pixel within the total swath, depending on its across-track position, is intercepted by the antenna footprint at a number of occasions, first in the forward direction and later in the backward direction. The radar operates in a pulsed mode, so that each point of the echo (time) profile can be attributed to a unique pixel position within the antenna footprint along the radial direction (range-gated).

[Chung-Chi.Lin@esa.int](mailto:Chung-Chi.Lin@esa.int); phone 31 71 5655813; fax 31 71 5654696; <http://www.esa.int>; European Space Agency (ESTEC), PO Box 299, 2200 AG Noordwijk, The Netherlands; \*\* [Ad.Stoffelen@knmi.nl](mailto:Ad.Stoffelen@knmi.nl); phone 31 30 2206585; fax 31 30 2210407; <http://www.knmi.nl>; KNMI, Postbus 201, 3730 AE De Bilt, The Netherlands; \*\*\* [wismann@ifars.de](mailto:wismann@ifars.de); phone 49 761 2851717; fax 49 761 2851719; <http://www.ifars.de>; Institute for Applied Remote Sensing, Am Josefsberg 2, 79100 Freiburg, Germany; \*\*\*\* [Sven.Bartha@astrium-space.com](mailto:Sven.Bartha@astrium-space.com); phone 49 7545 89309; fax 49 7545 82418; <http://www.astrium-space.com>; 88039 Friedrichshafen, Germany

In the above-mentioned study, a preliminary optimisation of the instrument parameters was performed based on simple design guidelines, driven mostly by:

- a large, useful swath-width exceeding 1500 km;
- the required spatial resolution;
- the required radiometric resolution across the swath for a specified minimum wind speed (signal-to-noise ratio of unity for minimising the radar average power at the minimum wind speed).

A simple, C-band, single polarisation (VV) system was presented as a result of a first iteration. It requires only a single passive antenna which size is comparable to the fore- (or aft-) antenna of ASCAT instrument (the latter has 6 antennas). A further step in elaborating the concept for improving the performance is to carry out end-to-end simulations of the complete system, starting with wind fields and attempting to recover the same fields by optimising the system parameters. Further sophistications of the system could be beneficial in improving the overall performance such as:

- use of dual-beam antenna instead of a fanbeam one for increasing the gain and to make a more homogeneous sampling across the swath;
- addition of a 2<sup>nd</sup> polarisation channel (HH);
- addition of a 2<sup>nd</sup> frequency channel (e.g. Ku-band);
- polarimetric radar for resolving directional ambiguity.

Hence, an RFSCAT simulator was developed which incorporates sufficient flexibility to model all those options.

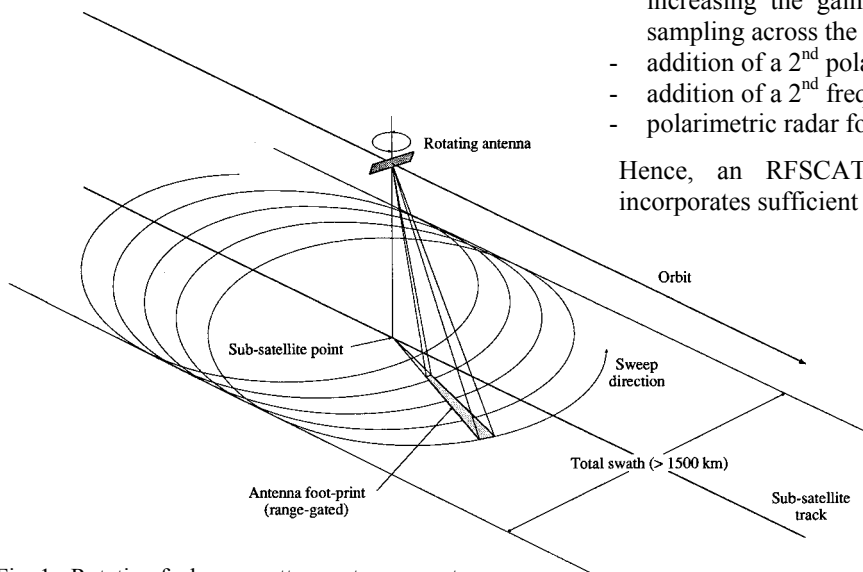


Fig. 1: Rotating fanbeam scatterometer concept

## 2. MEASUREMENT CHARACTERISTICS

### *Scan geometry and coverage*

The orbital spacecraft motion, combined with the regular fanbeam rotation, generates an epicycloidal footprint pattern on the Earth surface. The scan geometry depends on:

- the spacecraft (orbit) altitude;
- the antenna footprint size and position (with respect to the sub-satellite point);
- the antenna rotation speed.

The width of the total swath is determined by the farthest point of the antenna footprint. Generally, a largest possible swath is desirable according to the 2<sup>nd</sup> essential requirement mentioned above. This can be achieved by two means: (1) increase the orbit altitude for a given incident angle or; (2) increase the incident angle (range) for a given orbit altitude. The optimisation requires that the signal-to-noise ratio be maintained close to unity for the lowest required wind speed. As a consequence, the achievable swath width is constrained by the on-board power resource and the maximum allowable antenna size.

### *Number of acquisitions*

The inversion of the data to extract wind information requires at least 4 acquisitions at different azimuth view-angles during an over-flight. It is furthermore desirable that those azimuth view-angles are spaced not too close each others in order to limit the number of ambiguous solutions. Provision of a higher number of acquisitions (> 4) per over-flight could reduce the ambiguity problem by rendering the inversion over-deterministic, and also opens possibilities for other

applications such as sea-ice, snow and land observations.

In order to achieve a good coverage within the total swath and a large number of acquisitions, the rotation speed of the antenna must be sufficiently high such as to produce large overlaps of the antenna footprint between successive scans. If  $\omega_a$  (rad/s) is the rotation rate of the antenna, the satellite displacement  $\Delta x$  (km) between two successive scans (one complete rotation) is given by

$$\Delta x = v_g \frac{2\pi}{\omega_a} \quad (1)$$

where  $v_g$  is the spacecraft ground-speed ( $\cong 7$  km/s). This distance must be a fraction of the radial size of the antenna footprint. If e.g.  $\Delta x$  is one third of the latter, a point on the sub-satellite track is viewed 3 times in the forward direction and 3 more times in the backward direction during an over-flight.

The degree of overlaps depends on the across-track position and as a consequence, the number of acquisitions varies accordingly. An example of number of acquisitions per pixel as a function of its across-track position is shown in Fig. 2a. This result was obtained by simulating an over-flight over a line of pixels laid along the across-track direction and counting the number of interceptions by the antenna footprint. The following set of system parameters has been assumed for illustration purpose:

Orbit height:	725 km ( $v_g = 6.7$ km/s)
Total swath:	$\cong 1500$ km
Footprint length:	$\cong 410$ km (in radial direction)
Incidence angle:	$\cong 28^\circ - 51^\circ$
Antenna scan rate:	0.35 rad/s (3.3 rpm)

#### ***Incidence and azimuth view-angles***

The distribution of the incidence-angles as a function of the pixel across-track position is shown in Fig. 2b. For each of the pixel position, the local incidence-angle is displayed for all of the acquisitions during an over-flight. Note that the distribution is strongly dependent on the across-track position and converges to the highest value ( $51^\circ$ ) at the edges of the swath.

The distribution of the azimuth view-angles is depicted in Fig. 2c where angles are measured clockwise with respect to the satellite flight direction (opposite direction to the scan motion). Those angles are well-distributed between approximately 250 km to 700 km across-track distance which would result in well-behaving inversion of the GMF. Experience with SeaWinds data has shown that reliable wind inversion can actually be performed for pixels much closer to the sub-satellite track.

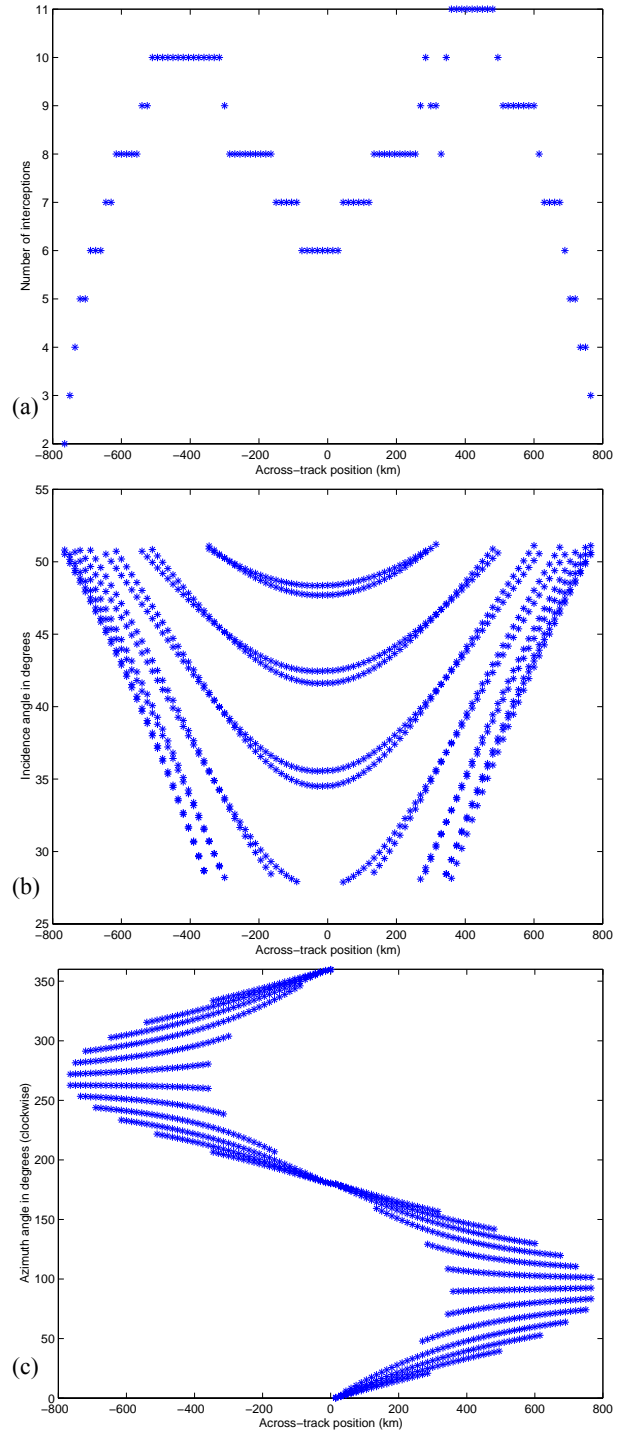


Fig. 2: (a) Example of number of interceptions; (b) Local incidence angles and (c) azimuth view-angles per pixel as a function of its across-track position

### **3. SCATTEROMETER SIMULATOR**

#### **3.1 Simulator overview**

The RFSCAT simulator is designed for the end-to-end performance analysis of wind field retrieval with the RFSCAT system. The simulation starts with an input wind field and a set of parameters defining the radar system and the applied processing. The output is a set of possible wind solutions for each grid point or so-called Wind Vector Cell (WVC). The difference between input wind field and output wind field are expressed as a Figure-of-Merit (FoM). The FoM is the metric used for the optimisation of the RFSCAT system.

For real existing scatterometer systems, the physics involved in the measurement can be described as follows:

- (1) A wind field generates surface waves on the ocean.
- (2) The scatterometer antenna sends a signal to the sea surface.
- (3) The signal is scattered by the sea surface.
- (4) The back-scattered signal is received by the scatterometer antenna.
- (5) The received signal is detected, on-board processed and down-linked to a ground station (level 0 data).
- (6) The level 0 data are transformed to physical units, calibrated and geo-located by the level 1 ground processor. The output is a level 1b product consisting of per-unit-surface backscattering coefficients  $\sigma^0$  and auxiliary data.
- (7) The level 2 processor computes the retrieved wind field (level 2 product) from the data of the level 1 product.

A strict simulation of steps (2) to (6) would imply that all systematic errors of the measurements have to be introduced to the simulated level 0 data and removed by the simulated level 1 processor afterwards. The objective of the RFSCAT system simulator is not the development of a level 1b processing algorithm, but the overall end-to-end performance evaluation. Therefore a more efficient approach with respect to run-time was implemented, applying the approximation that the level 1b processor is able to remove all significant systematic errors.

The simulation replaces steps (2) to (6) by the computation of the geometry, geo-location and variance of each measurement. These data are stored in a so-called „Pseudo-level 1 b product“. Given a specific wind field, the theoretical backscattering coefficient ( $\sigma^0$ ) for each measurement can be computed using the GMF. After the noise is added according to the variance, a level 1b product is generated and step (6) is reached.

Using the simulated level 1b product as input, the retrieved wind field is then computed by the level 2 processor (wind retrieval module).

The final processing step is the comparison of the input wind field with the retrieved wind field by the “Wind field Comparison Module”, resulting in the Figure-of-Merit.

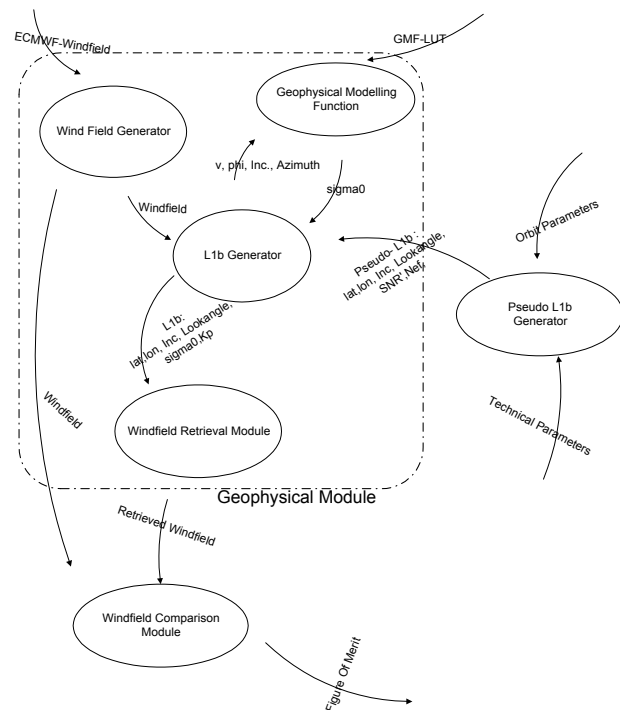


Fig. 3: Overall structure and data flow of the RFSCAT simulator

### 3.2 Wind-vector generator and geophysical model functions

#### Wind field

As input to the simulator, a spatially coherent wind field, or a systematic scan of the wind domain using discrete steps in the wind components (this resembles a uniform distribution over all wind vectors up to a certain maximum wind speed; see Fig. 4), or a set of random wind vectors representing a realistic global wind vector distribution can be selected providing full flexibility.

For testing of the RFSCAT concept, we follow the latter approach and create an artificial set of random wind vectors. Each wind component is chosen from a Gaussian distribution centred at 0 m/s and with a half width of 5.5 m/s. Since

the wind vectors are chosen at random, no spatial relation exists between them. In this way, it can be avoided that for example seasonal or local preferences in wind direction will cause a biased sampling of the wind distribution.

### **GMF**

The GMF, providing the normalised radar backscatter coefficient, depends on the measurement geometry (relative azimuth and incidence angle), sensing parameters (frequency, polarisation) and the wind vector. The GMF is a function devised to fit the available experimental data as good as possible. For the RFSCAT project the CMOD4 function for C-band VV-polarisation (both transmitting and receiving in vertical polarisation) is used<sup>3,4</sup>. This function has been used for operational wind retrieval for the ERS-2 Scatterometer data. For Ku-band, the NSCAT2 functions are used for VV and HH polarisation<sup>5</sup>. These functions have been used for the final reprocessing of all NSCAT data and is used at KNMI for SeaWinds processing. A GMF function for C-band HH-polarisation is not readily available. Therefore, it was estimated by scaling the CMOD4 function with the HH/VV ratio as defined by the NSCAT2 HH and VV functions. The estimated function is called CMOD4H.

GMF functions for polarimetric measurements at C and Ku-band do not yet exist. Therefore, a similar scaling procedure was necessary. The equations necessary to do this are given by Tsai et al.<sup>6</sup>. Furthermore a depolarisation ratio of -15dB, a symmetry factor of 0.5 and a signal attenuation of 1.0 were chosen. Using these formulas and assumptions, a new function called NSCAT2P was derived from the NSCAT2 functions, and a new function called CMOD4HP was derived from the CMOD4 and the CMOD4H functions. For reasons of computational efficiency, a look up table (LUT) is used to store the function values.

### **Geophysical noise contribution**

Geophysical noise is the effect of local variations of the wind inside the WVC. It has been experimentally found that this can be treated as an extra source of noise, on top of the noise produced by the instrument. The variabilities of the two types of noise should then be added to obtain the square of the total noise in the system.

It was found that the geophysical noise is a quadratic function of wind speed, increasing dramatically towards low wind speeds, and decreasing to practically zero (i.e. negligible compared to instrument noise) above 16 m/s (see Stoffelen<sup>7</sup> for a functional description). At 9 m/s, the geophysical noise is 3.2 % and at 3 m/s it increases to 10.9 %.

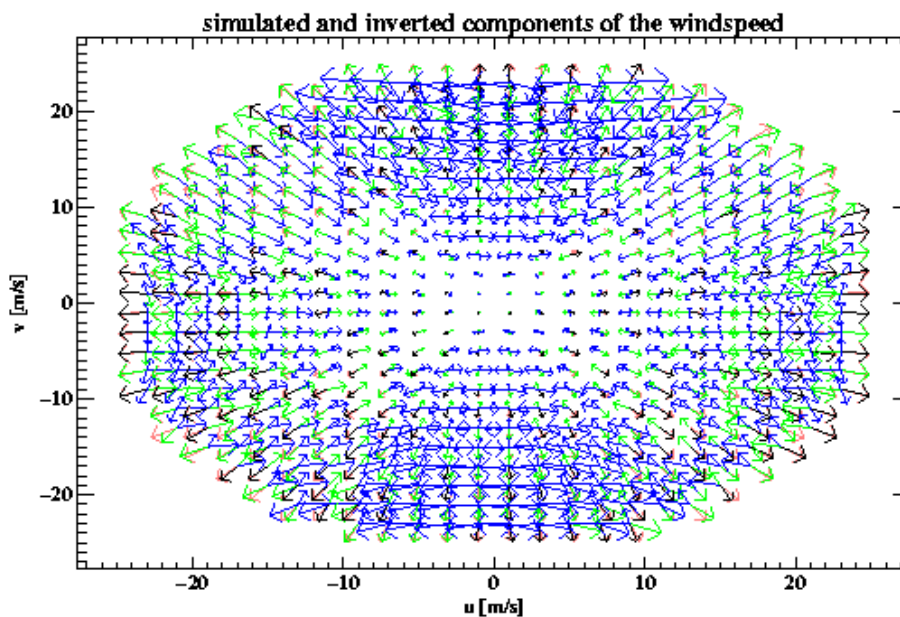


Fig. 4: Example of complete overview of simulated and inverted west-east (u) and south-north (v) components of the wind vectors. The true wind is red, retrieved closest wind ambiguity black, highest-ranked ambiguity green, and other ambiguities blue. Input wind field to the simulator was a wind vector set, binned in 1 m/s in both u and v direction.

### 3.3 Instrument simulator

#### Wind Vector Cells (WVCs)

The RFSCAT processing design is - similar to ERS and ASCAT- “WVC” oriented. The purpose of WVCs is to average many measurements by spatial filtering to one quantity with a low variance. The WVCs are on a (nearly) equidistant two-dimensional grid along the sub-satellite track and the plane perpendicular to the local ground track velocity (Fig. 5).

#### Samples

Samples represent measurements of the RFSCAT (Fig. 6). The signal of each sample represents an area on ground of the size of the effective spatial resolution of the instrument. The effective spatial resolution in the plane perpendicular to the antenna beam axis (azimuth) is a function of the antenna pattern and the measurement geometry.

The spatial resolution along the beam axis (range) is furthermore a function of pulse duration, the chirp rate and the local Doppler rate. The echo of each pulse results in a few thousand samples.

#### Views

Views are a collection of samples with similar azimuth angle belonging to one WVC (Fig. 7). For each view, the level 1b processor computes one sigma naught value by weighted averaging over its samples.

The number of views on a WVC depends on its location. WVCs on the sub-satellite track are seen under azimuth angle of 0° and 180° (two views), the WVCs in the far swath are seen under 90° or 270° (one view), while the WVCs in the mid-swath region are seen during the satellites over flight under many different azimuth angles (up to 10 views).

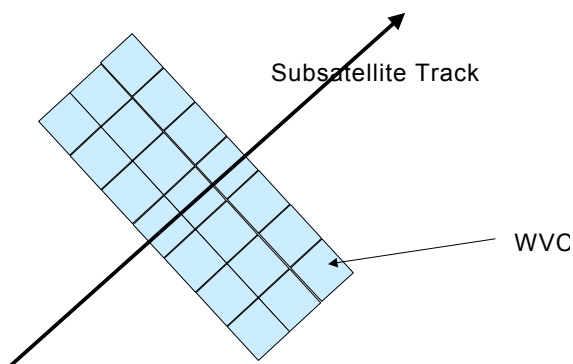


Fig. 5: Location of WVCs with respect to sub-satellite Track

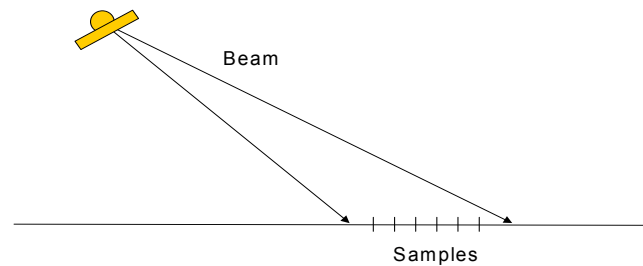


Fig. 6: The Echo of one Pulse results in many Samples

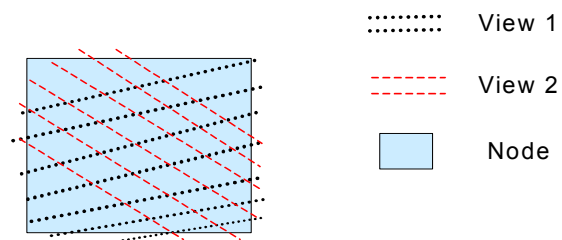


Fig. 7: The Picture shows one WVC with two Views

#### Pseudo level 1b simulation algorithm

For a given set of input parameters the pseudo level 1b generator computes the location of the WVCs, the number of views on each WVC and all quantities needed to compute for a given wind vector  $\sigma^0$  and its standard deviation. These are :

- (1) Latitude of WVC
- (2) Longitude of WVC
- (3) Incidence angle
- (4) Azimuth angle of antenna beam with respect to geographic north

- (5) Normalised  $SNR'$
- (6) Number of effective samples  $N^{eff}$
- (7) Polarisation

The quantities (1) to (4) are computed using an analytical orbit propagator (Kepler J2) and an ellipsoid Earth model.

The normalised signal-to-noise ratio  $SNR'$  per sample follows directly from the radar equation and  $SNR'$  per view results from the spatial filter applied on the view. The number of effective samples is the number of samples of a view corrected by their weight in the process of spatial filtering. Only samples from the same measurement modus may be collected to a view, therefore the polarisation is a view specific quantity, which may take the values VV, VH or HH. A further non-view-specific property of the instrument is the of number of noise measurements performed. This number results from the bandwidth of the noise measurement, the duration of the noise receive window and the number of receive windows used:

$$N^{noise} = B^{Noise} \cdot \tau^{rec} \cdot N^{Integration} \quad (2)$$

The level 1b generator computes the radiometric resolution  $K_p$  for each view, combining  $\sigma^0$  from the geophysical modelling function,  $SNR'$ ,  $N^{eff}$  and  $N^{noise}$ .

$$K_p = \sqrt{\frac{1}{N^{eff}} \left(1 + \frac{1}{SNR' \cdot \sigma^0}\right)^2 + \frac{1}{N^{noise}} \left(\frac{1}{SNR' \cdot \sigma^0}\right)^2} \quad (3)$$

Multiplication of the radiometric resolution with  $\sigma^0$  gives the standard deviation of the simulated measurement. Central Limit Theorem ensures that the random error of the measurement can be assumed to follow a Gaussian distribution.

### 3.4 Level 1b generator

The Level 1b (L1b) Generator is the part of the Geophysical module that calculates the simulated measurements and adds the noise to the measurements. In order to do this, it needs the wind vector provided by the wind field generator and the geometry calculated by the Pseudo L1b generator. The resulting simulated measurements are passed on to the wind field retrieval module. The L1b generator actually consists of the main loop of the Geophysical module. It loops over the WVC provided by the Pseudo L1b generator.  $K_p$  values are retrieved from the Pseudo L1b file, and the geophysical noise is calculated. Then Gaussian distributed noise is added to the simulated measurement (using the combined geophysical and instrumental noise). Finally the wind retrieval is carried out and the resulting wind vector ambiguities are stored. Some additional code was added to the main loop to perform the calculations for several wind vector cells in parallel; for this the MPI library is used.

### 3.5 Wind retrieval

The wind retrieval or inversion of the scatterometer data is done by the well-known algorithm that is used for the current as well as past scatterometer instruments (for example for ERS, NSCAT and SeaWinds on QuikScat). A maximum likelihood estimator (MLE) is calculated for a given geometry and simulated measurement using:

$$MLE = \sum_{views} \frac{(\sigma_{measured}^0 - \sigma_{tried}^0)^2}{K_p \cdot (\sigma_{measured}^0)^2} \quad (4)$$

with  $\sigma_{measured}^0$  the measured backscatter coefficient of a view,  $\sigma_{tried}^0$  the LUT value for the geometry of the current measurement, and for trial wind speed and direction,  $K_p (\sigma_{measured}^0)^2$ , a normalisation factor<sup>4</sup>. The two-dimensional wind domain (speed and direction) is scanned to find the local minima that are present in this plane. These give the set of wind vectors that give simulated  $\sigma^0$  values that best coincide with the measured ones.

The scanning of the wind domain is split in two parts. First for each wind direction (in fixed steps), the wind speed is scanned to find the wind speed having minimum MLE (see Fig. 8). It is known that in speed only one minimum should occur, simplifying the procedure. Starting from a first guess, the slope downhill (in MLE) is followed with given steps until the minimum is found. Then, if required, the steps are reduced in size, and the procedure is repeated using the found minimum as a starting point. If the steps have reached a specified minimum size the search is halted, and the

wind speed giving this minimum MLE is stored together with this minimum MLE value. The wind speeds giving minimum MLE at each wind direction (this is called the minimum valley in the wind domain) defines a curve as a function of wind direction, which is subsequently searched for local minima in MLE. The number of minima varies, and in special cases there may be just one, but usually 2 to 4 are found. The ambiguous solutions are sorted by MLE value, since the lowest MLE values correspond to a set of simulated NRCS that best fit the measurements.

The wind field retrieval (inversion) routine has been extensively tested using real data. This was done using measurements from SeaWinds on QuikScat, and comparing the result by the wind field retrieval routine, to the result of an older routine that is in use now for the operational processing of this data. From this comparison it was found that the new routine performs slightly better if the proper choices are made for stepping through the wind domain. This is at the expense of more computation time.

### 3.6 Figure-of-Merit function

For real scatterometer winds, heuristic methods exist to determine their quality<sup>8</sup>. These methods are based on experience and not fully objective. The problem of determining quality is caused by the ambiguous nature of the winds: multiple solutions exist with varying probability. Ranking scores and closest solution to reference wind vector RMS differences are used for validation, but these need to be combined in a FoM in order to provide a reasonable quality indication. To design future instruments, it may be appropriate to employ more fundamental ways of exploring wind quality and as such a new Figure-of-Merit (FoM) is derived. It is an objective score based on probabilistic arguments.

An objective quality measure is dictated by a specification. This specification is driven by the fact that the wind is largely a known quantity. The total dynamic range of wind components is governed by a standard deviation of about 6 m/s, whereas the required accuracy is about 1.5 m/s (see WMO<sup>9</sup>). This is a complication for designing an objective quality measure, i.e., ambiguities much outside the specification range are not bad, since these can be removed by using prior knowledge. However, those inside the specification range are clearly detrimental, as these can in real-life not be distinguished from each other and may cause detrimental impacts. A FoM is developed based on the product of a Probability-Density Function (PDF) encapsulating the prior knowledge and a PDF following from the ambiguous solutions. The FoM takes into account both uniqueness and accuracy properties of the RFSCAT winds.

## 4. SCATTEROMETER PARAMETER SETTING OPTIONS

The pseudo level 1b generator makes use the following input parameters:

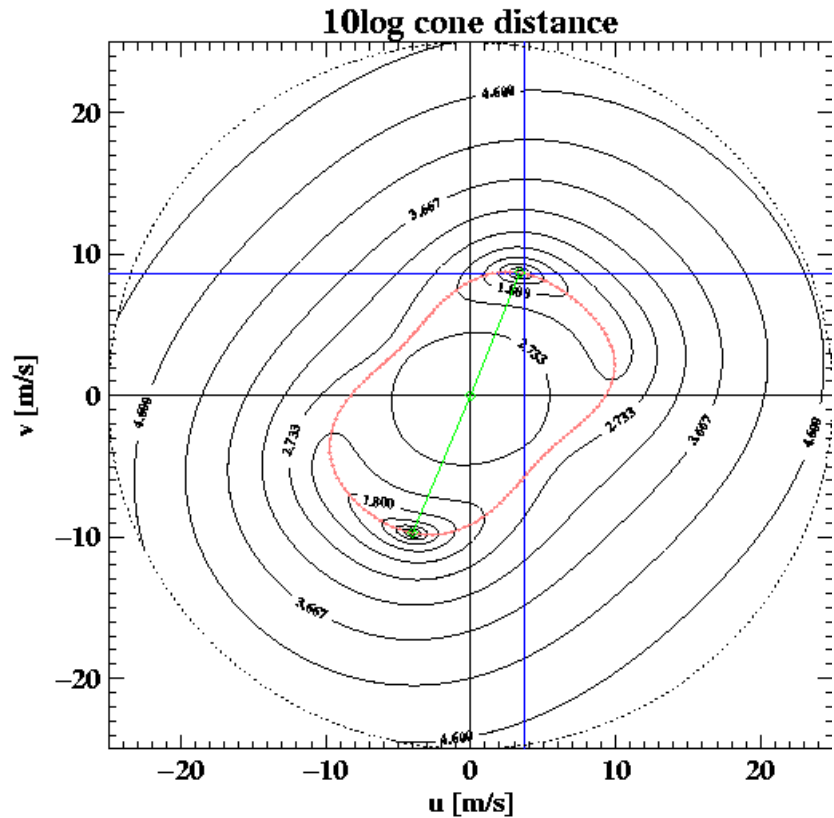


Fig. 8: The MLE function in the two dimensional wind domain (contours). The crossing blue lines indicate the input wind vector of the simulation. The red line indicates the minimum-valley (i.e. minimum MLE for each wind direction). The green vectors indicate the found wind solutions.

Duration and start date of simulated period
Osculating Keplerian elements of orbit
Antenna scan rate
Pulse repetition frequency
Transmit power
Tabulated two way antenna gain function
Wavelength
Losses within the instrument
Duration of transmit pulse
Chirp rate
-1.5 db width of antenna pattern in azimuth direction
Incidence angle dependent correction factor lowering antenna gain, to consider the rotation of the antenna during one measurement
Atmospheric losses
Reference temperature used to compute the noise power
Noise figure used to compute the noise power
Time offset from pulse transmit to opening of receive window
Length of receive window
Distance of WVCs
Tabulated spatial filter as a function of distance to the centre of WVC
Maximum allowed time difference for samples to be collected to one view
Bandwidth for noise measurements
Number of receive windows used for noise integration
Frequency of skipped pulse in order to perform noise measurements
Polarisation option

Table 1: List of input parameters for pseudo level 1b generator

## 5. SIMULATION RESULT

### *RFSCAT Simulations*

The wind retrieval performance of different options of RFSCAT instruments depends on the employed radar frequency and polarizations, and thus on the respective GMF as well as on the measurement geometry. The latter varies considerably across the swath of the instrument. For each node across the swath, the quality of the wind retrieval was estimated as described in Section 3, resulting in a curve for the FoM as a function of node number. An example is depicted in Fig. 9. The FoM is nearly symmetric around the center of the swath which is marked by the vertical line in the plot. The slight asymmetry is caused by different sampling on the right and left side of the swath due to different projected ground speeds of the footprint. The FoM for an entire simulation is defined as the mean value of the quality index across the entire instrument swath. This mean value is indicated by the horizontal line.

### *Simulator validation*

For validating the simulator software, the SeaWinds instrument aboard QuikScat has been simulated and the results were compared to measured data provided by the instrument. QuikScat measurement have been collected globally over a three days period and were processed to 100 km spatial resolution. The outer cells of the swath, which are known to provide winds of poor quality, were excluded. The simulation was done at 25 km spatial resolution for the

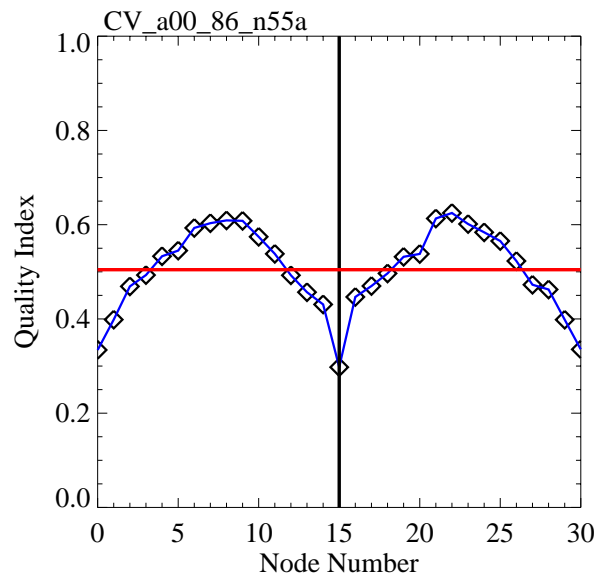


Fig. 9: Example of a FoM curve across the RFSCAT swath

entire 1800 km swath and is based on the technical parameters of the SeaWinds instrument. The result of the simulation together with the measured data is shown in Fig. 10. Except for nodes 59 and 63, there is very good agreement between measurement and simulation.

**Impact of SNR on retrieval performance**

The wind retrieval performance depends on the signal-to-noise ratio (SNR) for the  $\sigma^0$  estimates. In the course of designing an instrument, an optimum SNR across the entire swath and for the wide range of wind speeds and directions has to be found. Furthermore, ambiguities in the wind retrieval due to the shape of the GMF will limit additionally the wind retrieval performance. Instead of varying the entire set of instrument parameters affecting the SNR of the instrument, e. g., antenna peak gain, bandwidths, pulse peak power, only the transmitted peak power has been varied as a representative measure of the SNR while all others were kept constant. This may lead to unreasonable high power values for pulse peak power, but considering the potential in other design parameters these powers do not indicate an unrealistic instrument design.

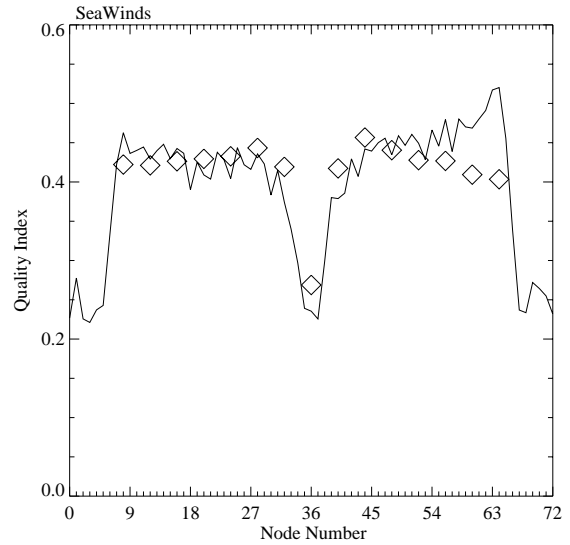


Fig. 10: FoM across the SeaWinds swath. For comparison data from an analysis of SeaWinds data are included (diamonds).

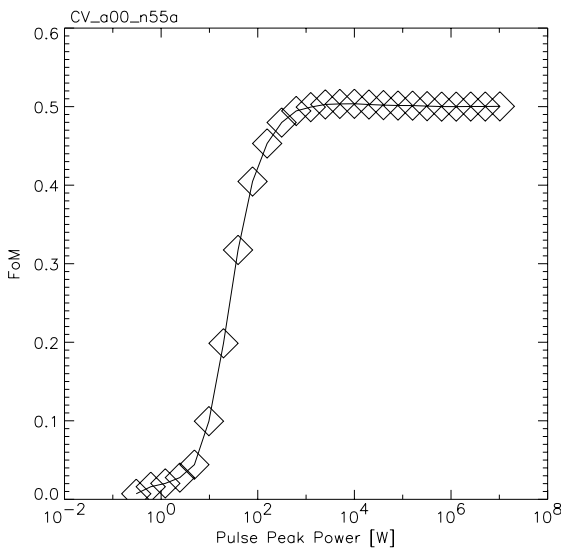


Fig. 11: FoM as a function of pulse peak power

region of the steep increase in FoM, but there is also no point in further improving the scatterometer beyond the point at which the FoM curves becomes flat.

**Impact of the antenna scan rate on retrieval performance**

Beside the SNR of the instrument the “azimuth sampling” of the  $\sigma^0$  measurements is affecting the wind retrieval performance. This sampling is being controlled by the antenna scan rate which directly influences the number of views per resolution cell and thus has an impact on the measurement geometry for each node. Fig. 12 depicts the relation between

Fig. 11 shows a typical example of the dependence of the FoM on the SNR represented by the transmitted pulse peak power. The quality of the retrieval increases significantly with SNR until a certain value of pulse peak power and then stays constant. From this point on the FoM is entirely controlled by the wind retrieval, which includes the corresponding geophysical model function (GMF) as well as the employed retrieval technique. From the technical and instrumental point of view, one would not want to operate the instrument in the

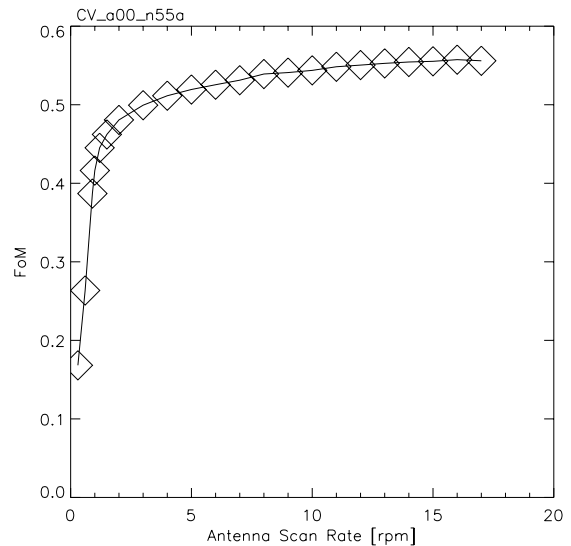


Fig. 12: FoM for the baseline instrument as a function of antenna scan rate.

FoM and antenna scan rate for the reference system used in this study.

Like for the SNR, the FoM increases with antenna scan rate due to the increased number of views for the wind retrieval and thus improved azimuthal separation between views. For scan rates higher than about 3 rpm, only very little information is being added by this “over-sampling”. From the respective graphs of the quality index as a function of node, it can be seen that the further slight improvement is found only around the center of the swath.

### System Comparisons

Within this study, various systems have been analysed. On the radar side, simulations were done for C and Ku-band for vertical (VV) and horizontal (HH) polarizations as well as for polarimetric cases. The measurement geometry includes low (725 km) and high (1075) orbits, narrow (1500 km) and wide (1800 km) swath width as well as low (50 km) and high (25 km) spatial resolution. Special emphasis was put on the analysis combinations of polarizations for the wind retrieval. Three typical examples are depicted in Fig. 13 which shows the simulation results for a C-band dual polarization instrument (a), a C-band polarimetric system (b) and a combination of a C and Ku-band vertically polarized scatterometer (c).

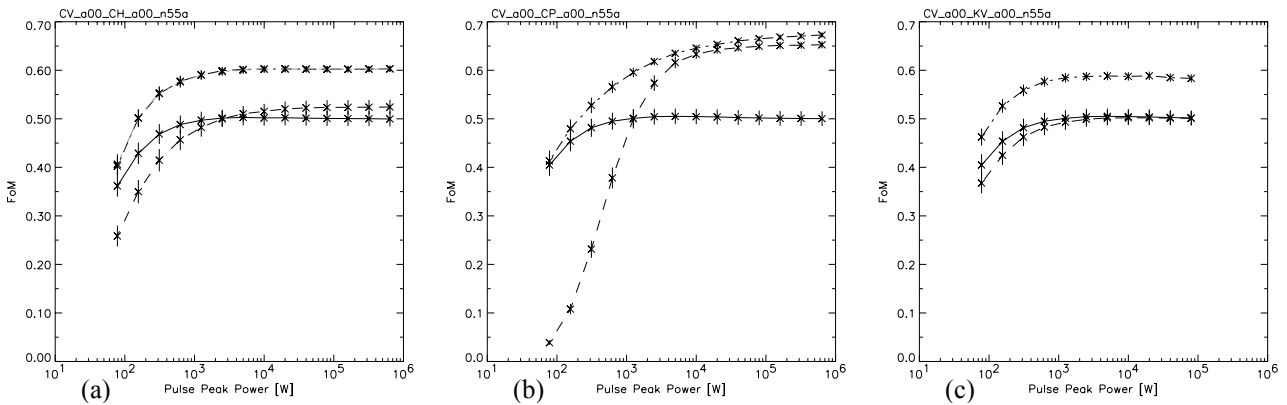


Fig. 13: FoM simulation results for: (a) a C-band dual polarization instrument; (b) a C-band polarimetric system; (c) a combination of a C- and Ku-band vertically polarized scatterometer. The solid line represents the C-band VV-polarization data. The dashed line shows the results for HH-polarization in (a), for polarimetric in (b), and for Ku-band VV-polarization in (c). The dashed-dotted line is for the respective combinations of the two channels. The error bars indicate the RMS variation of the FoM across the respective instrument swath.

Considerable differences between the systems are obvious from these graphs. They reflect very well differences between the radar channels, e.g., the SNR of the cross-polarized measurements required for the polarimetric mode is approximately 15 dB lower than the VV-polarization measurements (saturation attained at a much higher peak power). In general, a considerable improvement in wind retrieval can be achieved by combining channels. Especially, the polarimetric mode has a strong positive impact herein due to its capability of resolving wind direction ambiguities at the cost of high transmitter power.

In order to compare the different simulated systems each others, a reference performance point (RPP) is being computed on the respective FoM versus pulse peak power curve for each system. This point has the co-ordinates of a FoM being 10% below the saturation level of the curve and the corresponding pulse peak power. This reference point allows to relate the optimised scatterometer payload power to the achieved

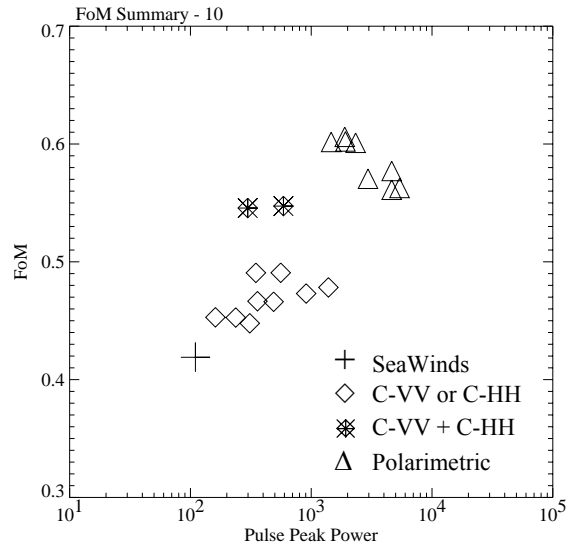


Fig. 14: Summary of reference performance points for various simulated systems.

performance in wind retrieval. A summary of RPP for system-options simulated so far is shown in Fig. 14. The result demonstrates that in general a two-channel system, i.e. 2-polarisation system (C-VV + C-HH) or 2-frequency system (C-VV + Ku-VV), performs better than a single-channel one (C-VV or C-HH). A polarimetric system performs best, but requires considerably more power. The figure demonstrates that a better wind retrieval performance comes at the expense of a higher instrument complexity. Such a parametric analysis is still on-going and will support system definitions and trade-offs for future windscatterometers. The goal is to arrive to a system which maximises the benefit-to-cost ratio for meeting the observation requirements<sup>9</sup>.

## 6. CONCLUSION

The next generation of windscatterometer will have to provide data of much improved quality and frequent global coverage in order to meet the ever-demanding requirements of NWP and very short-range forecasting. The RFSCAT concept presented herein could meet such requirements in a cost-effective manner. The present study addressed the development of a versatile end-to-end system simulator and a parametric analysis of various instrument configuration-options. The simulator is a flexible modelling tool which can accommodate a wide range of instrument configurations, choice of input wind field and various output options relating to the quality of the retrieved wind. It takes into account of the inherent geophysical noise in wind field as well as internally generated system noise (thermal noise and speckle noise).

The preliminary results of a parametric analysis shows that RFSCAT can provide better performance in comparison to the existing or soon-to-be-flown scatterometers both in terms of product quality and coverage performance (swath width). The system performance improves with increasing instrument complexity: a two-channel system (dual-polarisation or dual-frequency) performs better than a single-channel system; the polarimetric system performs best due to its capability to resolve wind-directional ambiguities, but is penalised by a very high power requirement. With regard to increasing the swath-width, an extension of the incidence range to a higher angle appears more beneficial than an increase of the satellite altitude. This is due to a better behaviour of the GMF at high incidence.

It must be remarked however that the validity of the results rely solely on the quality of the GMFs used in the simulations. Efforts are required to establish accurate model-functions for C-band HH, C-band polarimetric and Ku-band polarimetric cases.

## REFERENCES

1. L. Isaksen and A. Stoffelen, "ERS Scatterometer Wind Data Impact on ECMWF's Tropical Cyclone Forecasts," *IEEE Trans. Geoscience and Remote Sensing*, **38**, pp. 1885-1892, 2000.
2. C.C. Lin, B. Rommen, J.J.W. Wilson, F. Impagnatiello and P.S. Park, "An Analysis of a Rotating, Range-Gated, Fanbeam Spaceborne Scatterometer Concept," *IEEE Trans. Geoscience and Remote Sensing*, **38**, pp. 2114-2121, 2000.
3. A. Stoffelen and D. Andersen, "Scatterometer Data Interpretation: Transfer Function Estimation and Validation", *Journal of Geophysical Research*, **102(C3)**, pp. 5767-5780, 1997b.
4. A.C.M. Stoffelen, *Scatterometry*, Ph.D. Thesis, University of Utrecht, ISBN 90-393-1708-9, 1998, <http://www.library.uu.nl/digiarchief/dip/diss/01840669/inhoud.htm>
5. F.J. Wentz and D.K. Smith, "A model function for the ocean normalized cross section at 14 GHz derived from NSCAT observations", *Journal of Geophysical Research*, **104(C5)**, pp. 11499-11507, 1999.
6. Tsai et al., "Polarimetric Scatterometry: A promising technique for improving ocean surface wind measurements from space," *IEEE Transactions on Geoscience and Remote Sensing*, **38**, pp. 1903-1921, 2000.
7. A. Stoffelen, "Simulation of the Wind Performance of ASCAT," *OSI SAF Technical Note*, KNMI, De Bilt, 1998.
8. A. Stoffelen, J. de Vries, A. Voorrips, "Towards the real-time use of QuikScat winds", *Beleidscommissie Remote Sensing*, Report No. USP-2/00-26.
9. World Meteorological Organisation, SatRep-26, Geneva, 2002, <http://www.wmo.ch>.